Alma Mater Studiorum Università di Bologna
Archivio istituzionale della ricerca

Features and application of coupled cold plasma and photocatalysis processes for decontamination of water

Features and application of coupled cold plasma and photocatalysis processes for decontamination of water

Annachiara Berardinelli[a,b], Abdessalem Hamrouni[c], Sandra Dirè[a], Riccardo Ceccato[a], Giovanni Camera-Roda[d], Luigi Ragni[e,f], Leonardo Palmisano[g], Francesco Parrino[a*]

[a] Department of Industrial Engineering, University of Trento, Via Sommarive 9, 38123 Trento, Italy;

[b] Centro Agricoltura Alimenti Ambiente – C3A, University of Trento, Via E. Mach 1, 38010 S. Michele all'Adige (TN), Italy;

[c] Laboratoire de Recherche Catalyse et Matériaux pour l'Environnement et les Procédés URCMEP (UR11ES85), Faculté des Sciences de Gabès/Université de Gabès, Campus Universitaire Cité Erriadh, Gabès 6072, Tunisia;

[d] Department of Civil, Chemical, Environmental, and Materials Engineering, University of Bologna, via Terracini 28, Bologna (40131), Italy;

[e] Dipartimento di Scienze e Tecnologie Agro-Alimentari, University of Bologna, Piazza Goidanich 60, 47521 Cesena (FC), Italy;

[f] Interdepartmental Centre for Agri-Food Industrial Research, Alma Mater Studiorum, University of Bologna, Via Quinto Bucci, 336, 47521 Cesena (FC), Italy;

[g] Dipartimento di Ingegneria, University of Palermo, Viale delle Scienze Ed. 6, Palermo (90128), Italy.

*Correspondence: mail: francesco.parrino@unitn.it; tel: +39 0461 285295

Abstract

Dielectric barrier discharge plasma and photocatalysis have been proposed as tools for decontamination of process water, especially in food industry. The present investigation aims to redefine and identify the features of coupling the two technologies in terms of degradation efficiency of a model compound. Results show that, when the process is carried out in plasma activated water in the presence of irradiated TiO_2, the efficiency of the integrated process is lower than the sum of the two processes acting separately. It is proposed that afterglow species, e.g. hydrogen peroxide and/or peroxynitrites could be activated by UVA light irradiation producing hydroxyl radicals in the liquid phase. Even if TiO_2 limits this additional effect by acting as UVA screen barrier material, its decontamination efficiency under certain conditions results higher than that obtained with plasma systems. These results open the route to chlorine-free decontamination processes and redefine the application framework of this integrated approach.

1. Introduction

The decontamination of fresh cut fruits and vegetables poses several safety issues and is challenging due to the huge amount of drinking water needed (ca. 40 m^3 per ton of product). In fact, these products are generally eaten uncooked, and contamination could occur during different production steps (Meireles et al., 2016). Chlorine is widely applied to this aim, but it does not generally afford mineralization of residual antibiotics and/or pesticides eventually present and, worse still, produces carcinogenic and mutagenic chlorinated compounds which then accumulate in the process water.

Different alternative approaches, mainly based on advanced oxidation processes, were deeply investigated (Barbosa-Cánovas et al., 2017, Bhilwadikar et al., 2019). Among them, as witnessed by the increasing number of published researches, the use of cold plasma under atmospheric conditions could combine decontamination efficiency, process safety, and the need to preserve the organoleptic features of the products (Berardinelli et al., 2016). In fact, glowing plasma discharge above the aqueous phase to be decontaminated (plasma activated water, PAW) (Shen et al., 2016) has been proposed as a viable alternative to chlorine based sanitizers. Various devices working in different conditions (direct current, low frequency, radio frequency and microwave discharges), with peculiar geometries, energy demand, and in the presence of various gas mixtures can be used to drive the discharge. Among the low frequency plasma sources, Dielectric Barrier Discharge (DBD) devices are, undoubtedly, the most investigated and industrialized non-equilibrium plasma generators. In a DBD device the discharge is driven by applying alternating current between two electrodes often characterized by a separation gap of few millimetres and by one or more dielectric layers. DBD presents relevant advantages in terms of costs, flexibility, operating parameters (air as medium, frequency and voltage), due to its simple and versatile electrode geometry (planar or circular) and its ability to produce a stable discharge with negligible thermal effects (Tang et al., 2018). Moreover,

2

the separated configuration between electrodes and PAW limits corrosion phenomena, and avoids

contamination of water with heavy metals easily occurring in underwater systems such as plasma jet

devices, which are therefore unsuitable for food applications. Finally, the DBD plasma device is

known to produce higher amount of active species with respect to plasma jet glow discharges (Leduc

et al., 2010) due to its larger surface area. Reactive species are generated through collision

mechanisms in the gas phase. When air is used as working gas to generate non-equilibrium plasma

discharges, reactive oxygen species (ROS) and reactive nitrogen species (RNS) are formed. Ozone

(O_3), atomic oxygen (O) and hydroxyl radical ($OH^.$) are the main ROS, while excited molecules of

N_2 and nitrogen oxide radicals are the main RNS characterizing a non-equilibrium plasma (Ragni et

al., 2010). Many authors investigated reactions involving these species in gas phase (Du et al., 2008,

Misra et al., 2016, Moreau et al., 2016, Yousfi et al., 2011) or in liquid phase for underwater devices

(Lukes et al, 2012, Sun et al., 2012, Tian et al., 2014). However, the interaction of plasma generated

in gas phase close to a liquid medium, and the distribution of active species in the liquid phase is less

understood (Jiang et al., 2016), although this information is crucial to understand and control the

decontamination capability of the system. Active species generated by the plasma discharge can

directly diffuse through the gas/liquid interface, or can be generated in the liquid phase by post-

discharge chemical reactions (Bruggeman et al., 2016, Zhou et al., 2018, 2016). The complexity of

this scenario has been mainly approached by numerical simulation techniques which allowed to

estimate mass transfer kinetic and other relevant parameters. For instance, numerical simulation

performed by Yusupov et al. (2013) showed that ROS possessed high penetrating power into a 500

molecule thick water layer. Liu et al. (2016) investigated the role of the air gap between the plasma

and the liquid medium and concluded that for gaps larger than 0.5 cm the concentration of active

species in the PAW steeply decreases. In almost all the experimental investigations the pH value of

the PAW reduces up to 3 - 3.5 after few minutes of discharge (Liu et al., 2010, Moreau et al., 2007).

The concentration of reactive species in the liquid phase depends on several factors such as the system

configuration, treatment time, discharge gap, carrier gas, applied voltage, and the electron energy

87 (Gurol et al., 2012, Pavlovich et al., 2013, Tian et al., 2015). In a recent review, it has been reported

88 that ozone, hydrogen peroxide, nitrite, nitrate, superoxide ions, and peroxynitrite are the active

89 species mainly present in PAW (Perinban et al., 2019).

90 Heterogeneous photocatalysis is one of the most studied advanced oxidation processes for

91 environmental purposes (Parrino et al., 2019). TiO_2 is widely used as the photocatalyst in these

92 applications due to its low cost, non-toxicity, stability and high activity. Briefly, under irradiation of

93 suitable wavelength, electrons and holes are generated in the conduction and valence bands of TiO_2,

94 respectively. Interfacial electron transfer with species adsorbed to or in proximity of the surface of

95 TiO_2 induces formation of highly oxidizing radical species such as hydroxyl, superoxide, nitrate

96 radicals and singlet oxygen (Parrino et al., 2018), which are mainly responsible for the degradation

97 and mineralization of pollutants (Hamrouni et al., 2020) and for inactivation of pathogens such as

98 bacteria, fungi, algae, viruses and microbial toxins (Kumar and Bansal, 2013, Zhu et al., 2018). In

99 particular, TiO_2 photocatalysis has been used for the disinfection of washing water coming from fresh

100 vegetables industry towards natural microflora and potentially pathogenic microflora (Selma et al.,

101 2008). Others research experiences refer about the bactericidal photocatalytic activity of TiO_2 on

102 carrots (Cho et al., 2007) and iceberg lettuce (Kim et al., 2007) with respect to both washing water

103 and vegetables decontamination.

104 TiO_2 photocatalysis has been often integrated with other purification techniques such as biological

105 treatments (Parrino et al., 2019b), adsorption onto activated carbons (Cataldo et al., 2016), ozonation

106 (Camera-Roda et al., 2019), membrane separation (Toledano Garcia et al., 2018), among others.

107 Combination of cold plasma and photocatalysis is mainly reported for air purification systems. In

108 these cases, synergistic effects between the two technologies have been observed, mainly justified by

109 invoking the well-known synergy between TiO_2 photocatalysis and ozone (Parrino et al., 2013). For

110 instance, synergistic effects have been observed for the degradation of isovaleraldehyde (Palau et al.,

111 2015) and butyraldehyde (Gharib-Abou et al., 2016) in gas phase. Coupled photocatalysis-plasma

112 systems have been also applied for smoking rooms air deodorization (Ochiai et al., 2012), hospital

4

113 indoor air decontamination (Zadi et al., 2018), oxidation of mixtures of pollutants (Vorontsov et al.,

114 2012), and reduction of CO_2 into CO and O_2 at low temperatures (Mei et al., 2016).

115 On the other hand, only few researches deal with DBD plasma-photocatalysis systems for the

116 decontamination of liquid media. In most of these applications the plasma discharge is generated

117 underwater using point to plane geometry electrodes. The degradation of model pollutants such as

118 phenol, 4-chlorophenol, or tetracycline occurred faster than the single processes in most of the cases

119 when TiO_2 was suspended (He et al., 2014) or deposited on supports (Lukes et al., 2005). Similar

120 results have been obtained in such systems also for the inactivation of E. Coli by using microplasma

121 jet arrays and N_2, He, O_2 and air as the working gases (Zhou et al., 2016b). Only few reports deal

122 with the degradation of pollutants in liquid phase below the DBD plasma discharge acting in the head

123 space. For instance, Aziz et al. (2018) coupled different oxidation processes with DBD plasma in a

124 planar falling film reactor, and compared the integrated processes in terms of energy yield. Ghodbane

125 et al. (2014) reported on the degradation of the anthraquinone dye Acid Blue 25 by using DC glow

126 discharge and TiO_2 photocatalysis. However, in these reports the term synergy has been often used

127 to indicate a general increase of efficiency with respect to photocatalysis or plasma, but not with

128 respect to their sum. Moreover, as demonstrated by Camera Roda and Santarelli (2007) when synergy

129 between two processes exists, it depends primarily on the ratio between the rate of the two processes

130 operating separately under the same experimental conditions. This result, often disregarded, allowed

131 in this work to clarify the problem of synergy between TiO_2 photocatalysis and DBD plasma in non-

132 submerged systems, by rationally approaching the intensification problem.

133

134 **2. Material and methods**

135 Figure 1 schematically shows the discharge chamber. The external walls of the chamber were made

136 of Pyrex in order to allow external irradiation as below detailed.

137

5

138
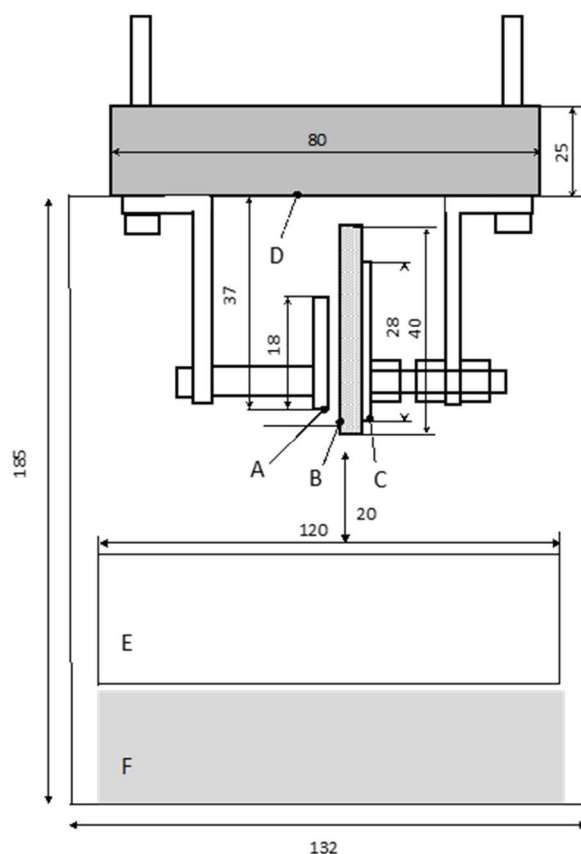
Figure 1. Layout of the discharge chamber. A: cathode; B: glass plate; C: anode; D: fan; E: Pyrex
reactor; F: magnetic stirrer. The reported values of dimensions are in millimetres.

141

The degradation of methylene blue (MB, Sigma-Aldrich, St. Louis, Mo, USA) was used as model
reaction to evaluate the decontamination efficiency of the system. 200 mL of magnetically stirred
MB aqueous solution (0.02 mM, if not otherwise specified) was placed in a Pyrex cylindrical reactor
(inner diameter 120 mm; height 60 mm) positioned within the chamber. The free surface of the
solution was ca. 20 mm below the gas plasma discharge. The discharge was generated by using a
dielectric barrier discharge (DBD) device characterized by two parallel plate electrodes made of brass
($28 \times 12.6 \times 4.7$ mm) and stainless steel ($18 \times 9.9 \times 5.5$ mm), respectively. The brass electrode was
covered by a thin sheet of glass ($40 \times 14.6 \times 0.05$ mm) working as dielectric barrier. Inside the
chamber, a fan mounted at about 37 mm from the bottom of the stainless steel electrode was placed
in order to direct the afterglow species towards the free surface of the methylene blue aqueous
solution.

6

153   The discharge was driven by high voltage transformers and power switching transistors supplied by

154   a stabilized DC power supply (Elektro-Automatik GmbH & Co.KG, Viersen, Germany, EA-PS 2042-

155   06B) placed outside the chamber. Input voltage of 19.15 V (3.15 ± 0.5 A) and air as working gas were

156   considered.

157   The voltage output was characterized by a like-shaped sinusoidal waveform with a peak to peak value

158   of 13.8 kV (frequency around 46 kHz).

159   The concentration of MB during the treatments was measured by means of a Shimadzu UV-vis

160   spectrophotometer (Kyoto, Japan) which measured the absorbance at 663 nm of samples withdrawn

161   during the runs at fixed intervals of times. TiO_2 P25 (Evonik, Essen, Germany; specific surface area

162   56 $m^2 \cdot g^{-1}$, 93% anatase, 7% rutile) was used as the photocatalyst for selected runs in amounts ranging

163   from 0.01 to 1 $g \cdot L^{-1}$ (Bellardita et al., 2017, 2018). Selected runs have been performed from 3 to 5

164   times and the reproducibility was better than 5%.

165   Irradiation was performed by means of six actinic Mercury UV-A lamps (Philips, Eindhoven, The

166   Netherlands; nominal power 14 W each, with emission peak at 365 nm) surrounding the chamber in

167   a hexagonal geometry. The radiation intensity of each lamp was ca. 7 $W \cdot m^{-2}$, as measured at the

168   reactor wall point nearest to the lamp by means of a Delta Ohm DO9721 radiometer equipped with a

169   UVA probe. After 10 minutes of plasma treatment the temperature inside the glass chamber reached

170   33 ± 1°C   (starting from ca. 26 °C) and was constant during the treatment. The chemical

171   characterization of the atmosphere within the chamber in the presence of the discharge has been

172   elsewhere reported (Ragni et al., 2016).

173   Tests to unveil the role of peroxynitrite and hydrogen peroxide have been performed according to the

174   following procedures. Detection of H_2O_2 in the reacting mixture was performed by the titanium

175   peroxide method (Wolfe, 1962). Briefly, 5 mL of $TiCl_4$ (Sigma Aldrich, p.a.) were added to 5 ml of

176   a 6M aqueous solution of HCl at ice temperature and then diluted to 500 mL in 6M HCl. Aliquots of

177   this solution were added to the sample and the absorbance of the yellow titanium peroxo complex

178   (measured by means of a Shimadzu UV-vis spectrophotometer, Jasco V-570, Japan) was used to

7

179 check the presence of hydrogen peroxide. Peroxynitrite standard solutions were prepared by mixing

180 1 mL of sodium nitrite (0.3 M, Sigma Aldrich, p.a.), 1 mL hydrogen peroxide (0.7 M, Sigma Aldrich,

181 p.a.) and 0.5 mL of hydrochloric acid (0.6 M, Sigma Aldrich, 37%) as aqueous solutions. 0.5 mL of

182 an aqueous solution of sodium hydroxide (1.5 M, Sigma Aldrich, p.a.) was immediately added within

183 2-3 seconds to stabilize the solution. Nitrite ion was the limiting reactant, and to eliminate the excess

184 of H_2O_2, the solution was mixed with MnO_2 (Sigma Aldrich p.a.), left under stirring for 20 minutes,

185 and filtered. MB was added to the solution and the pH was adjusted to ca. 2 by adding HCl. Finally,

186 the solution was kept in the dark for 20 minutes and irradiated under UVA light (10 W UV LED,

187 supplied by GraceLightLed) for 5 minutes. The concentration of MB during the tests was measured

188 by UV-vis spectroscopy (Jasco V-570, Japan). Benzoic acid (Sigma-Aldrich, p.a.) has been used as

189 a molecular trap to highlight the presence of hydroxyl radicals in the reacting mixture, by monitoring

190 the formation of salicylic acid through fluorescence spectroscopy (λ_{exc}= 270 nm, Jasco FP-6300,

191 Japan).

192

193 **3. Results and discussion**

194 Preliminary photocatalytic experiments were carried out at a fixed initial MB concentration by

195 changing the amount of TiO_2 and keeping constant the other experimental conditions. Results are

196 represented by symbols in Figure 2A. Experimental data have been fitted by using Eq. 1, as the

197 photocatalytic degradation of MB proceeds according to first order kinetics (Salehi et al. 2012).

198 $r = -\dfrac{dC_{MB}}{dt} = k_{obs}C_{MB}$ (1)

199 where r is the reaction rate, C_{MB} the concentration of MB, and k_{obs} the observed apparent kinetic

200 constant. The values of the initial MB concentration and of k_{obs} have been obtained by fitting the

201 experimental concentration vs. time data by the least squares method. As it is evident the model

202 satisfactorily fits the experimental data. The obtained values of k_{obs} are reported in Figure 2B against

203 the TiO_2 amount suspended in the photocatalytic medium.

204

205
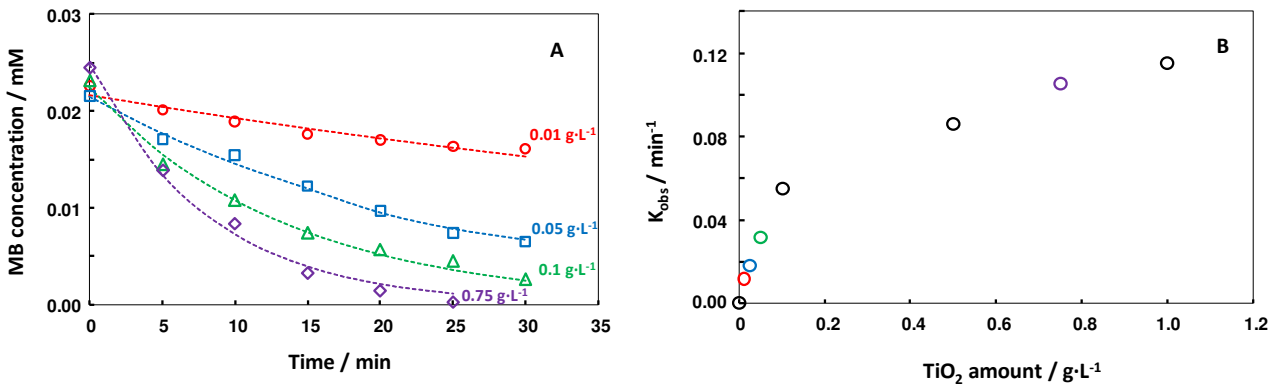
Figure 2. MB photocatalytic degradation during irradiation time, for some representative runs carried

out in the presence of different concentrations of TiO_2 (Panel A). The observed kinetic constants have

been reported in Panel B against the amount of TiO_2 dispersed in the photocatalytic medium.

A linear behavior of the observed kinetic constant (see Eq. 1) for the photocatalytic reaction rate

against the photocatalyst amount is apparent up to TiO_2 concentrations of ca. 0.1 g·L^{-1} (see Panel B),

while the curve tends to a plateau for higher TiO_2 amounts. The mechanism of the photocatalytic

degradation of MB is well known, and readers are referred to the relevant literature for details (Dariani

et al. 2016). Briefly, irradiating TiO_2 under UV light results in the formation of electron-hole pairs

(Eq. 2). Highly oxidizing hydroxyl radicals, formed upon reduction of oxygen (Eq. 3-5) and water

oxidation (Eq. 6), along with other reactive oxygen species (ROS) such as singlet oxygen (Eq. 7)

(Parrino et al., 2018) are, in turn, mainly responsible for the degradation of MB.

$$TiO_2 + h\nu \rightarrow TiO_2^*(e^-; h^+) \tag{2}$$

$$O_2 + e^- + H^+ \rightarrow HO_2^{\cdot} \tag{3}$$

$$2\ HO_2^{\cdot} \rightarrow H_2O_2 \tag{4}$$

$$H_2O_2 + e^- + H^+ \rightarrow OH^{\cdot} + H_2O \tag{5}$$

$$H_2O + h^+ \rightarrow OH^{\cdot} + H^+ \tag{6}$$

$$TiO_2^*(e^-; h^+) + {}^3O_2 \rightarrow TiO_2 + {}^1O_2 \tag{7}$$

9

225

226   We would like to stress here that the use of dyes should be avoided in photocatalysis when testing

227   novel photocatalysts under visible light irradiation (Yan et al., 2006). In fact, the complex

228   photochemistry of MB (Mitoraj et al. 2018) and the substrate dependent nature of photocatalysis (Ryu

229   and Choi, 2008, Parrino et al. 2017) could produce results of difficult interpretation. Moreover,

230   indirect photocatalytic mechanisms triggered by the excited triplet state of the dye could mask the

231   real activity of the photocatalytic material. In this case, however, TiO_2 is the main light absorbing

232   species due to the fact that the irradiation wavelength (centered at 365 nm) matches its absorption

233   band, and that at this wavelength range MB shows low absorption capability. Therefore, indirect

234   photocatalytic paths can be neglected in these conditions. Accordingly, blank tests performed by

235   irradiating MB solutions in the absence of TiO_2 did not result in appreciable MB degradation within

236   the considered time range.

237   In order to investigate the coupling between plasma treatment and photocatalysis, we performed the

238   photocatalytic degradation of MB under external UV light irradiation and in the presence of TiO_2, by

239   simultaneously switching on the plasma discharge within the system. Results are represented in

240   Figure 3 by the curve labelled as PL@PC@UV. Figure 3 reports also the MB degradation due to the

241   sole photocatalysis (PC@UV curve) and to the plasma treatment under simultaneous UV light

242   irradiation (PL@UV curve). Notably, all of the three runs reported in Figure 3 have been carried out

243   under UV irradiation, for the sake of comparison.
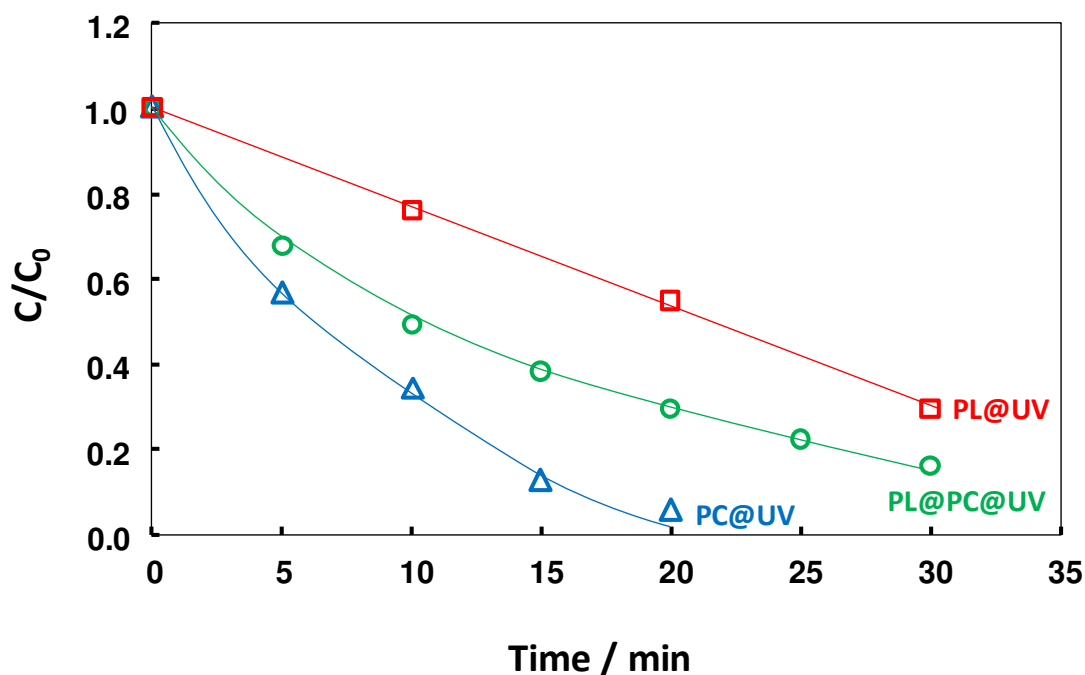
Figure 3. Normalized concentration of MB during reaction time for some representative runs of sole photocatalysis (PC@UV, blue triangles), plasma-UV (PL@UV, red squares), and plasma-photocatalysis (PL@PC@UV, green circles). Initial MB concentration C_0 = 0.02 mM, TiO_2 amount for the photocatalytic runs 0.75 g·L^{-1}.

Under the given experimental conditions, the degradation rate of MB due to the sole photocatalysis is faster than the one induced by plasma and UV light. However, surprisingly, the MB degradation obtained when coupling plasma and photocatalysis is slower than that of photocatalysis alone, even if it is higher with respect to that of plasma and UV light. This implies that in this case the two technologies not only do not show any synergistic effect, but the simultaneous use of plasma and photocatalysis is detrimental with respect to the sole photocatalysis.

These results do not agree with those reported in literature in which, generally, the integration of plasma and photocatalysis results in process intensification. It is worth mentioning that low energy DBD plasma has been poorly investigated in literature and integration with photocatalysis has been carried out in gas phase but never in the head space above a photocatalytic liquid suspension as in this case. The reported synergy between plasma and photocatalysis for the degradation of model

11

compounds in gas phase, such as butyraldehyde and isovaleraldehyde, (Palau et al., 2015, Gharib-

Abou et al., 2016) has been justified by assuming that the ozone produced by plasma was the main

oxidant, and that its concomitant action with the irradiated TiO_2 increased the degradation rate with

respect to the sum of the single technologies (Camera-Roda et al., 2017). In fact, in the presence of

ozone only 1 electron (1 photon) is required to produce one OH radical (Eq. 8-9), while 3 electrons

(3 photons) are necessary in the presence of oxygen (Eq. 3-5).

$$O_3 + e^- + H^+ \rightarrow HO_3^{\cdot} \qquad\qquad (8)$$

$$HO_3^{\cdot} \rightarrow O_2 + OH^{\cdot} \qquad\qquad (9)$$
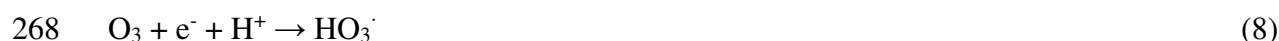
The evident absence of synergy expressed in Figure 3 can be due to different reasons.

First of all, the diffusion of ozone from the gas phase (where it is generated) to the liquid phase could

limit the process. The ozone diffusion coefficient has been estimated by Jiang et al. (2013) being 1.75

$\cdot 10^{-5}$ $cm^2 \cdot s^{-1}$. Ozone can effectively oxidize MB at the gas-liquid interface or even within the first

liquid layers, but its action can be limited by mass transfer within the bulk of the solution. Notably,

in the present experimental set up only gentle magnetic agitation could be performed, as at higher

agitation speeds formation of water droplets within the electrodes destabilized the discharge.

As demonstrated in the relevant literature (Parrino et al., 2013), the synergy between photocatalysis

and ozone is dependent on the ratio between the rates of the single technologies. This aspect is

generally disregarded, whereas it might explain why in some cases the values of the intensification

factors measured by different researchers are very dissimilar. Therefore, in principle, opposite results

could be obtained also in this case by changing the rate of one of the two processes. In order to check

this hypothesis, we measured the MB degradation rate in the plasma-photocatalysis integrated system

at different TiO_2 concentrations. The apparent observed kinetic constants were determined

differentiating the experimental data at the initial time, by using a five points formula for equally

286   spaced points (Yeow et al., 2003, Lubansky et al., 2006). The obtained k_{obs} values versus the amount

287   of TiO_2 for the plasma-photocatalysis integrated process are reported in Figure 4.
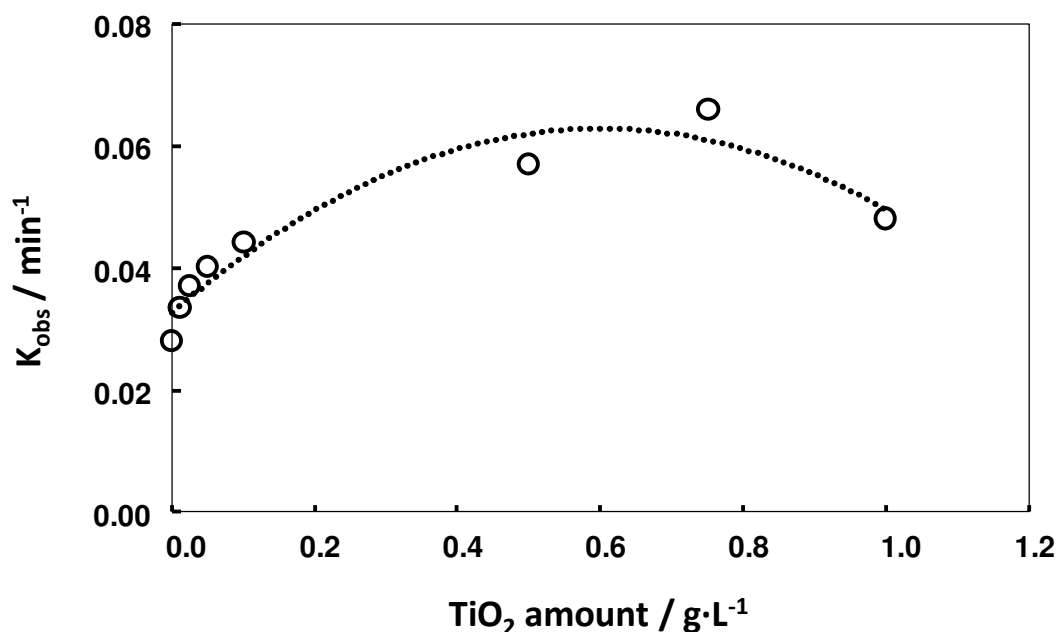
288

289

290   **Figure 4.** Observed kinetic constants calculated at the initial time against the amount of TiO_2

291   for integrated runs with plasma and photocatalysis.

292

293   It is apparent that the initial rate of degradation of MB, proportional to the k_{obs} values, during the

294   coupled plasma-photocatalytic process increases with the amount of photocatalyst until a maximum

295   is reached. Thereafter, for TiO_2 concentrations higher than ca. 0.5-0.7 $g \cdot L^{-1}$ the rate of the integrated

296   process decreases. The presence of a maximum indicates the existence of an optimum at which

297   photocatalysis and plasma can be used at the highest efficiency. On the other hand, such a behavior

298   is the typical result of two contrasting processes operating simultaneously during the integrated

299   process. As above reported (Figure 2B) the rate of photocatalysis increases until a plateau is reached.

300   Therefore, a second process, related to the plasma discharge and/or with UV light irradiation, must

301   contribute to MB degradation and its efficiency is supposed to decrease with increasing catalyst

302   loading.

303   In order to evidence the nature of this second process, it is useful to define the following integration

304   factor (E_i) as in Eq. 10

305

306    $$E_i = \frac{k_{obs}(PC@PL@UV)}{k_{obs}(PC@UV) + k_{obs}(PL@UV)}$$ (10)

307

308   Where $k_{obs}(PC@PL@UV)$ is the observed rate constant of the integrated plasma-photocatalysis

309   process, while $k_{obs}(PC@UV)$ + $k_{obs}(PL@UV)$ is the algebraic sum of the rate constants of

310   photocatalysis and plasma-UV processes. In other words, E_i expresses at which extent the integrated

311   process is more (if $E_i > 1$) or less effective (if $E_i < 1$) with respect to the sum of the two processes

312   acting separately. In Figure 5 is reported the trend of the integration factor (E_i) at increasing TiO_2

313   amounts.
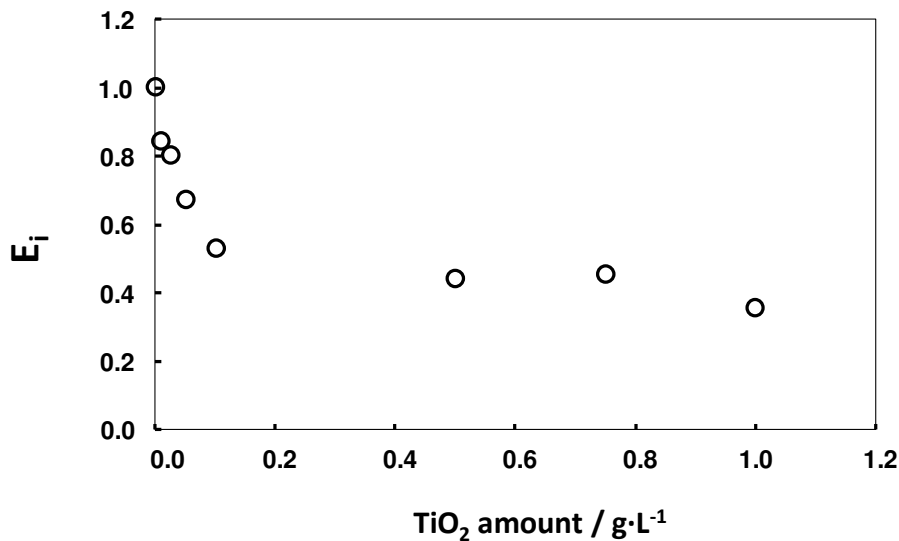
315   **Figure 5.** Trend of the integration factor E_i at increasing concentration of TiO_2

316

317   In the absence of photocatalysts, E_i is equal to 1 by definition. By increasing the amount of TiO_2, the

318   integrated process is progressively less efficient than the sum of the two processes until, at a TiO_2

319   concentration of ca. 0.2 $g \cdot L^{-1}$, a plateau is reached. Two conclusions can be drawn from these results:

320   (i) a negative synergy is observed between plasma and photocatalysis under these conditions; (ii) the

14

ozone induced oxidation process, known to provide a positive synergy when coupled with photocatalysis, plays a minor role when photocatalysis acts together with DBD plasma.

The detrimental effect of TiO_2 on the plasma induced MB degradation is necessarily due to the interaction between TiO_2 and some species generated by the discharge which then dissolve in the reacting suspension. In this regard, it should be noted that the pH of the solution changed from around 6 to 3 within the first 15 minutes of discharge and UV-vis spectra of the solutions showed the presence of nitrate and nitrite ions according to literature (Ragni et al., 2016).

Blank photocatalytic tests of MB degradation performed in the presence of nitrate and nitrite ions, while maintaining constant the other conditions, did not show significant differences, indicating that these ions, generated upon the plasma discharge, are not directly responsible for the observed behavior. Regardless of their nature, the oxidizing species produced by the plasma discharge are deactivated by the presence of TiO_2. This can occur by interaction of these species with the photogenerated charges at the surface of TiO_2, or simply because TiO_2 acts as UV light screen, thus reducing their direct photochemical activation. If the second hypothesis holds, the extent of the effect of plasma during photocatalysis should be dependent on the portion of the reactor effectively irradiated. In fact, the higher is the concentration of TiO_2, the lower is the penetration of the light and the smaller is the volume of the reactor where irradiation is effective.

To tackle this issue, for each photocatalyst concentration we calculated the mean free photonic path (i.e. the radius of the reactor annulus well irradiated, at which the optical thickness is equal to 1) as the ratio between the radius of the reactor and the optical thickness. Note that the optical thickness is equal to the specific extinction coefficient of TiO_2 P25 at 365 nm ($5.8 \cdot 10^4$ $cm^2 \cdot g^{-1}$) multiplied by the photocatalyst concentration and by the radius of the reactor (Satuf et al., 2005). In this way it is possible to estimate the percentage of the photoreactor effectively irradiated ($\%V_{irr}$) at each photocatalyst concentration. Results are reported in Figure 6.
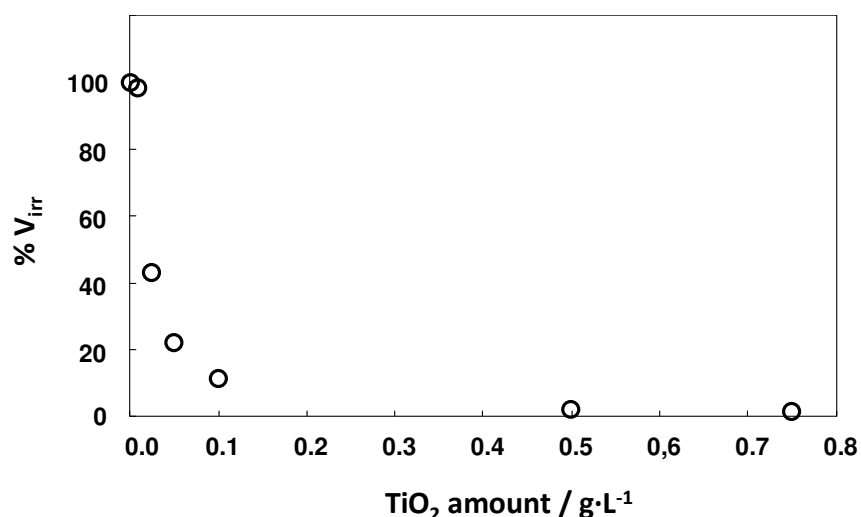
Figure 6. Percentage of reactor volume effectively irradiated at different TiO_2 concentrations of the suspension.

Results show that in the absence of the photocatalyst the whole volume is effectively irradiated ($\%V_{irr}$ = 100), while increasing the photocatalyst concentration results in a steep decrease of the portion of volume effectively irradiated until, for TiO_2 amounts higher than ca. 0.2 $g \cdot L^{-1}$, the decrease is negligible and a plateau is reached. It is evident that while the rate of photocatalysis reaches a plateau for TiO_2 concentrations higher than 0.75 $g \cdot L^{-1}$ (Figure 2B), the trend of the integration factor E_i (Figure 5) is similar to that of the percentage of volume well irradiated (Figure 6), as it reaches a plateau at ca. 0.2 $g \cdot L^{-1}$. This evidence supports the hypothesis that TiO_2 simply acts as a screen during the integrated plasma-photocatalysis process and that some of the photoactive species produced by the discharge are simply activated by UV light.

As a further proof of the existence of UV light absorbing species generated by the plasma discharge and contributing to MB degradation, we performed the plasma treatment in the absence of TiO_2, with and without UV light irradiation. Results are shown in Figure 7.

16
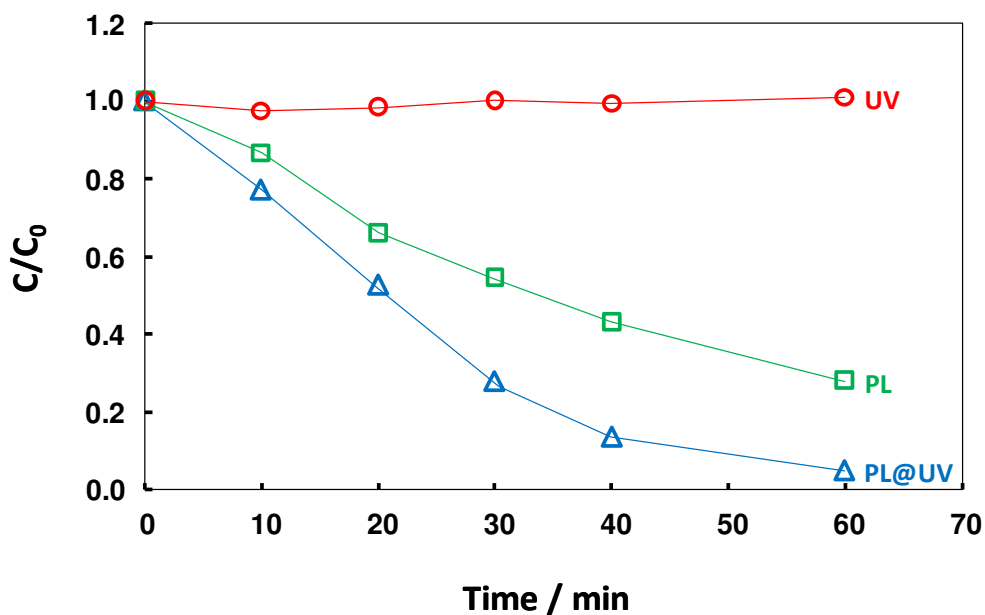
Figure 7. Normalized concentration of MB during time for runs performed under sole UV light irradiation (red circles, UV), by the sole plasma discharge treatment (green squares, PL), and by plasma discharge treatment performed under simultaneous UV light irradiation (blue triangles, PL@UV).

It is evident that UV light alone does not induce MB degradation. Contrarily, plasma discharge in the absence of external UV light irradiation results in ca. 40% degradation of MB after 30 minutes of irradiation, while the degradation reached ca. 70% in the same time when the solution is externally irradiated. This result confirms that the plasma discharge produces species that are activated by UV light. To unravel the mechanism underlying this effect, we checked the presence of OH radicals in the irradiated and non-irradiated suspensions in the presence of the plasma discharge. We perform the experiments by only substituting MB with benzoic acid, under otherwise identical conditions. In fact, in the presence of OH radicals, benzoic acid is hydroxylated to salicylic acid according to Eq. 11.
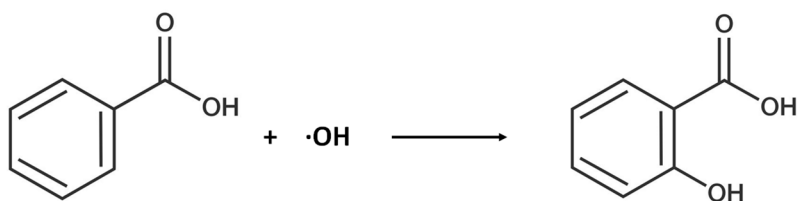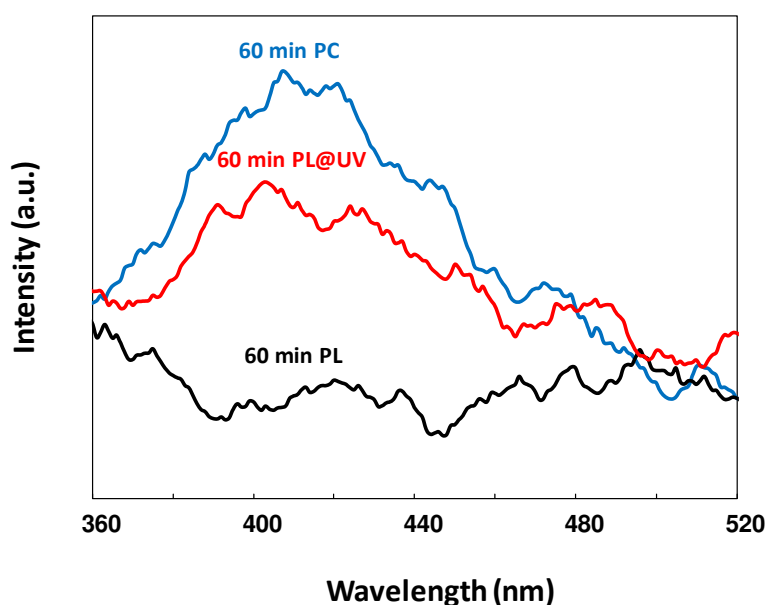
378 (11)

379 The presence of salicylic acid has been detected by measuring its fluorescence at 410 nm. Results are

380 shown in Figure 8.

381

382

383 **Figure 8.** Fluorescence spectra of samples of reacting suspension for runs carried out in the

384 presence of 0.5 mM of benzoic acid after 60 minutes of plasma treatment (black curve), of plasma

385 under external UV light irradiation (red curve), and of photocatalytic treatment without plasma and

386 with 0.1 g·L^{-1} TiO$_2$ (blue curve). Excitation wavelength: 270 nm.

387

388 Notably, a quantitative comparison of the spectra was not possible due to the influence of the different

389 treatments on the composition of the suspension. However, it can be seen that salicylic acid could be

390 detected in the presence of irradiated TiO$_2$ (blue curve), and in the presence of the plasma discharge,

391 only if the solution was externally irradiated. On the contrary, salicylic acid was virtually absent when

392 the plasma treatment was performed under dark conditions.

18

393 Formation of hydroxyl radicals by means of photocatalysis is well documented and occurs according

394 to Eqs. 2-6.

395 The absence of hydroxyl radicals when the solution was treated by plasma under dark conditions is

396 reasonable, by considering that hydroxyl radicals eventually formed in the discharge zone could not

397 live enough to reach the bulk of the solution beneath. In fact, the life time of OH radicals is reported

398 to be in the order of magnitude of microseconds (Perinban et al., 2019).

399 On the other hand, when plasma discharge was performed under external UV irradiation, the

400 formation of salicylic acid could be detected, thus indicating that hydroxyl radicals are responsible

401 for the enhanced MB degradation observed when plasma was performed under UV irradiation with

402 respect to the dark conditions.

403 This finding justifies the previously observed detrimental behaviour of TiO_2 when plasma and

404 photocatalysis simultaneously operated. In fact, photochemical reactions triggered by UVA light

405 absorbing species must be the responsible for the observed formation of hydroxyl radicals.

406 Direct detection of these species was not straightforward at this step of research, by considering their

407 possible transient nature. However, some hypotheses can be proposed, while further investigation are

408 ongoing to afford definitive proofs.

409 OH radicals could form from hydrogen peroxide (Cataldo, 2014) which undergo photolysis at any

410 wavelength lower than 380 nm with a quantum yield Φ ranging between 1 and 1.5, according to Eq.

411 12.

412

413 $H_2O_2 + h\nu \rightarrow 2\ OH^{\cdot}$ (12)

414

415 However, during plasma treatment the amount of H_2O_2 in the liquid phase was lower than the

416 detection limit (1 μM) of the method based on titanium peroxocomplexes described in the

417 experimental part. On the other hand, as the absence of evidence is not evidence of absence, it cannot

418 be excluded that hydrogen peroxide could be present at lower concentrations or for times shorter than

419 those of analysis. In fact, the presence of hydrogen peroxide has been often reported in similar

420 systems, even if at concentrations closer to the detection limit (Ragni et al., 2016).

421 Nitrate ions photolysis could be excluded as a source of hydroxyl radicals as photons below 300 nm

422 (required for this reaction) are cut off by Pyrex glass (Parrino et al., 2016).

423 The presence of nitrite ions in solution with MB under UV irradiation did not result in MB

424 degradation. Therefore, nitrite ions alone are not responsible for the observed production of hydroxyl

425 radicals.

426 Peroxynitrite ion is reported among the species that can be present in the aqueous phase below the

427 plasma discharge (Tarabová et al., 2019). Peroxynitrite ($ONOO^-$) can be formed by reaction of

428 superoxide and nitric oxide radicals (Eq. 13) formed after glow (Goldstein and Merényi, 2008).

429 Notably the life time of the superoxide radical is long enough (ca. 5 seconds) in aqueous solution and

430 is easily protonated to hydroperoxyl radical at pH lower than 4.8 (Eq. 14) (Bielski et al., 1985).

431

432 $O_2^{\cdot-} + NO^{\cdot} \rightarrow ONOO^-$ (13)

433 $O_2^{\cdot-} + H^+ \rightarrow HO_2^{\cdot}$ (14)

434

435 Moreover, peroxynitrite can be formed by reaction of nitrite and hydrogen peroxide according to Eq.

436 15 (Saha et al., 1998).

437

438 $H_2O_2 + NO_2^- \rightarrow ONOO^- + H_2O$ (15)

439

440 By considering that the pH of the MB solution is acidic (ca. 3), it is probable that peroxynitrite is

441 present in its protonated form in solution. In fact, pKa of peroxynitrous acid is ca. 6.8. Peroxynitrous

442 acid is a highly oxidizing and nitrating agent. It is rather unstable with respect to its corresponding

443 anion, and it easily undergoes homolytic rupture to NO_2 and hydroxyl radical. By considering that

444 the peroxynitrite shows an absorption band with a maximum at 302 nm which can extends up to 390

445   nm, it is possible that production of hydroxyl radicals could be sped up under UVA irradiation.

446   Coddington et al. (1999) report the formation of hydroxyl radicals by decomposition of peroxynitrite

447   ions in aqueous solution. Beckman et al. (1990) observed that peroxynitrite rapidly decomposes once

448   protonated with a half-life of 1.9 s at pH 7.4 thereby generating a strong oxidant with reactivity similar

449   to hydroxyl radical. Khan at al. (2000) reported the decomposition of peroxynitrite to nitroxyl anion

450   and singlet oxygen. However, Martinez et al. (2000) soon later observed that formation of singlet

451   oxygen could be observed only in the presence of traces of hydrogen peroxide. Most of the reports

452   concern the behaviour of peroxynitrite under dark conditions, while few is known about its

453   photochemical behaviour. Recently Thøgersen et al. (2015) investigated the primary photochemistry

454   of peroxynitrite aqueous solutions irradiated at 266 nm by transient absorption spectroscopies. More

455   than 90% of the peroxynitrite was dissociated after 400 ps and the dominant path was the formation

456   of superoxide anion radical and nitrogen monoxide. To the best of our knowledge the effects of

457   radiation at longer wavelengths have been poorly investigated. To the aim of our work, it was

458   interesting to ascertain if UVA irradiation could affect the degradation of MB in the presence of

459   peroxynitrite ions and/or hydrogen peroxide. Further investigation is ongoing in order to detail the

460   mechanistic aspects of this behaviour.

461   Figure 9 shows the normalized concentration of MB under dark and under UVA irradiation in the

462   presence and in the absence of peroxynitrite ions. Notably, the pH of the as prepared standard solution

463   was ca. 12. Blank tests allowed to determine that MB degradation, at this pH value, proceeded both

464   under dark conditions and (faster) under UVA irradiation even in the absence of peroxynitrite.

465   Therefore, the tests in Figure 9 have been performed by acidifying the solution containing MB at pH

466   ca. 3 (i.e. the pH of the MB solution under plasma discharge) by means of HCl (0.7 M solution)

467   addition prior to starting the test.

468
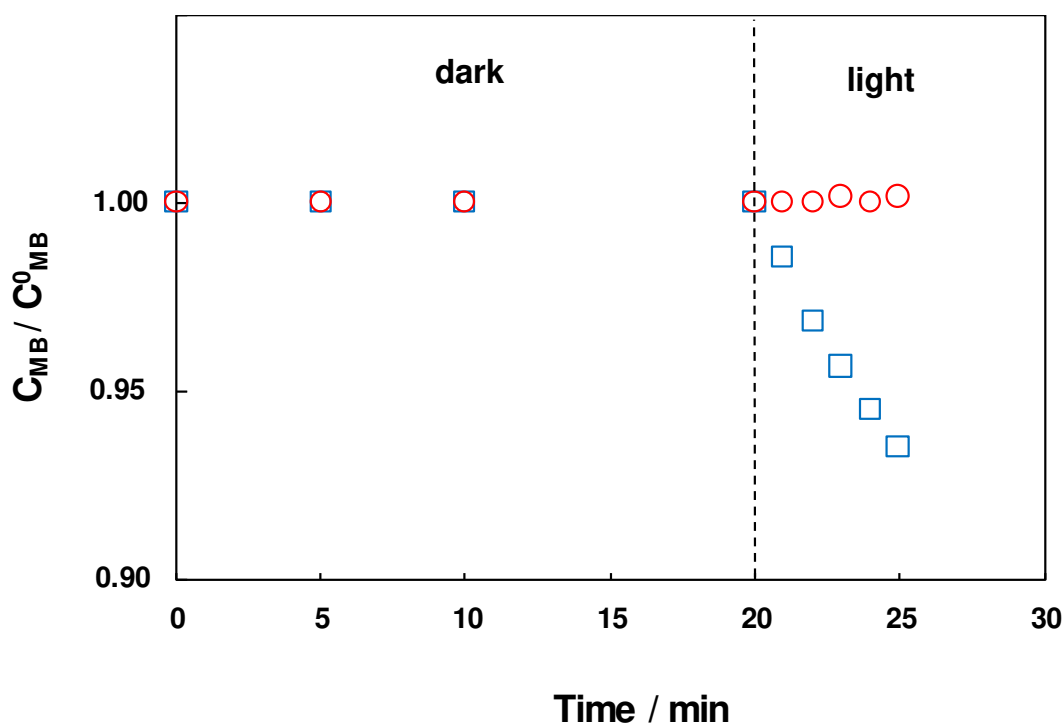
Figure 9. Normalized concentration of MB versus time in acidified (pH = 3) peroxynitrite standard

solution (blue squares) and in the absence of peroxynitrite (red circles) under dark and under UV

light irradiation.

Addition of HCl resulted in an immediate drop of MB concentration, possibly due to direct

peroxynitrous acid formation that induced oxidation (not shown in Figure 9). Thereafter, the MB

concentration was stable under dark and the pH was constant at ca. 3. The solution was maintained

in the dark for twenty minutes and the concentration of MB did not decrease as it is evident from

Figure 9. However, under UVA irradiation the concentration of MB decreased of ca. 8% after 5

minutes in the presence of peroxynitrite, while remained constant in its absence.

Blank tests performed in the absence of peroxynitrite but in the presence of H_2O_2 afforded similar

results (not shown). Even if hydrogen peroxide was removed from the peroxynitrite solution by

passing it through powdered MnO_2, and its concentration was monitored by the titanium peroxide

method, the presence of H_2O_2 at concentration lower than the detection limit cannot be excluded in

the present experimental conditions. However, the present tests suggest that peroxynitrite and/or

485 hydrogen peroxide could be tentatively proposed as the active species responsible for the enhanced

486 MB degradation observed when plasma discharge acts under UVA irradiation.

487

488 **4. Conclusions**

489 The interaction between photocatalysis and the plasma discharge generated above the liquid

490 suspension by means of a DBD device, has been investigated by monitoring the degradation of

491 methylene blue in the aqueous phase as a model reaction. Results showed an optimum in the

492 efficiency of MB degradation obtained by coupling plasma and photocatalysis exists for TiO_2

493 concentrations of ca. 0.5 $g \cdot L^{-1}$. This bell behaviour, however, indicates the existence of two

494 contrasting processes simultaneously acting during the integrated process. In fact, increasing the

495 amount of TiO_2 results in higher photocatalytic activity but, at the same time is detrimental as far as

496 the joint effect of plasma and photocatalysis is concerned. In fact, the efficiency of the integrated

497 process with respect to the sum of the two processes acting separately decreases with increasing the

498 TiO_2 concentration in the reacting mixtures. This finding has been related with the production of

499 active species absorbing UVA light which in turn generate hydroxyl radicals in the aqueous solution,

500 as demonstrated by fluorescence spectroscopy. Accordingly, in the absence of TiO_2, irradiating the

501 aqueous solution above which the plasma is glowed enhances the degradation rate of MB with respect

502 to the simple use of plasma. Experimental results show that peroxynitrous acid and/or hydrogen

503 peroxide generated upon the action of plasma could be responsible for the observed behaviour.

504 Notably, due to the substrate dependent nature of photocatalytic reactions, further investigation in the

505 presence of different pollutants is required to obtain a full picture of the complex interplay between

506 plasma and photocatalysis. However, these preliminary results define the terms of interaction between

507 plasma and photocatalysis and show that the integration of these technologies under opportune

508 conditions could be a promising alternative to the use of chlorine for the disinfection of fresh cut

509 vegetables in the food processing chain.

510

511 **Competing interest statement**

512 The authors have no competing interests to declare.

513

514 **References**

515 Aziz, K.H.H., Miessner, A., Müller, H., Mueller, S., Kalass, D., Khorshid, I., Rashid, M.A.M., 2018.
516 Application of a planar falling film reactor for decomposition and mineralization of methylene blue
517 in the aqueous media via ozonation, Fenton, photocatalysis and non-thermal plasma: A comparative
518 study. Process Saf. Environ. Prot. 113, 319-329. https://doi.org/10.1016/j.psep.2017.11.005

519 Barbosa-Cánovas, G.V., Donsi, F., Pokhrel, P.R., Candoğan, K., Guadarrama-Lezama, A.Y., 2017.
520 Nonthermal stabilization processes, in: Roos, Y.H., Livney, Y.D. (Eds.), Engineering Foods for
521 Bioactives Stability and Delivery, Springer, New York, pp. 341–360.

522 Beckman, J.S., Beckman, T.W., Chen, J., Marshall, P.A., Freeman, B.A., 1990. Apparent hydroxyl
523 radical production by peroxynitrite: Implications for endothelial injury from nitric oxide and
524 superoxide. Proc. Natl. Acad. Sci. USA. 87, 1620-1624. https://doi.org/10.1073/pnas.87.4.1620
525
526 Bellardita, M., El Nazer H.A., Loddo V., Parrino F., Venezia A.M., Palmisano, L., 2017.
527 Photoactivity under visible light of metal loaded TiO_2 catalysts prepared by low frequency ultrasound
528 treatment. Catal. Today 284, 92–99. http://dx.doi.org/10.1016/j.cattod.2016.11.026
529
530 Bellardita, M., Di Paola, A., Megna, B., Palmisano, L., 2018. Determination of the crystallinity of
531 TiO_2 photocatalysts. J. Photochem. Photobiol. A: Chem. 367, 312-320.
532 https://doi.org/10.1016/j.jphotochem.2018.08.042
533
534 Berardinelli, A., Pasquali, F., Cevoli, C., Trevisani, M., Ragni, L., Mancusi, R., Manfreda, G., 2016.
535 Sanitisation of fresh-cut celery and radicchio by gas plasma treatments in water medium. Postharvest
536 Biol. Technol. 111, 297–304. https://doi.org/10.1016/j.postharvbio.2015.09.026
537
538 Bhilwadikar, T., Pounraj, S., Manivannan, S., Rastogi, N.K., Negi, P.S., 2019. Decontamination of
539 microorganisms and pesticides from fresh fruits and vegetables: a comprehensive review from
540 common household processes to modern techniques. Comp. Rev. Food Sci. F. 18, 1003-1038.
541 https://doi.org/10.1111/1541-4337.12453
542
543 Bielski, B.H.J., Cabelli, D.E., Arudi, R.L. Ross, A.B., 1985. Reactivity of HO_2/O_2^- Radicals in
544 Aqueous Solution, J. Phys. Chem. Ref. Data 14, 1041-1100. https://doi.org/10.1063/1.555739
545
546 Bruggeman, P.J., Kushner, M.J., Locke, B.R., Gardeniers, J.G.E., Graham, W.G., Graves, D.B.,
547 Ceriani, E., 2016. Plasma–liquid interactions: A review and roadmap. Plasma Sources Sci. T. 25,
548 053002. https://doi.org/10.1088/0963-0252/25/5/053002
549
550 Camera-Roda, G., Loddo, V., Palmisano, L., Parrino, F., 2019. Photocatalytic ozonation for a
551 sustainable aquaculture: A long-term test in a seawater aquarium. App. Catal. B: Environ. 253, 69-
552 76. https://doi.org/10.1016/j.apcatb.2019.04.048
553

Camera-Roda, G., Loddo, V., Palmisano, L., Parrino, F., Santarelli, F., 2017. Process intensification in a photocatalytic membrane reactor: Analysis of the techniques to integrate reaction and separation, Chem. Eng. J. 310, 352-359. https://doi.org/10.1016/j.cej.2016.06.019

Camera-Roda, G., Santarelli, F., 2007. Intensification of water detoxification reactors made easy by considering the photons as immaterial reactants. J. Sol. Energy Eng. 129, 68–73. https://doi.org/10.1115/1.2391204

Cataldo, F., 2014. Hydrogen peroxide photolysis with different UV light sources including a new UV-LED light source. NEW FRONT. CHEM. 23, 99-110.

Cataldo, S., Iannì, A., Loddo, V., Mirenda, E., Palmisano, L., Parrino, F., Piazzese, D., 2016. Combination of advanced oxidation processes and active carbons adsorption for the treatment of simulated saline wastewater. Sep. Purif. Technol. 171, 101-111. https://doi.org/10.1016/j.seppur.2016.07.026

Cho, M., Choi, Y., Park, H., Kim, K., Woo, G.J., Park, J., 2007. Titanium dioxide/UV disinfection in fresh carrots, J. Food Prot. 70, 97-101. https://doi.org/10.4315/0362-028x-70.1.97

Coddington, J.W., Hurst, J.K., Lymar, S.V., 1999. Hydroxyl radical formation during peroxynitrous acid decomposition. J. Am. Chem. Soc. 121, 2438-2443. https://doi.org/10.1021/ja982887t

Dariani, R.S., Esmaeili, A., Mortezaali, A., Dehghanpour, S., 2016. Photocatalytic reaction and degradation of methylene blue on TiO_2 nano-sized particles, Optik 127, 7143-7154. https://doi.org/10.1016/j.ijleo.2016.04.026

Du, C.M., Sun, Y.W., Zhuang, X. F., 2008. The effects of gas composition on active species and byproducts formation in gas–water gliding arc discharge. Plasma Chem. Plasma P. 28, 523–533. https://doi.org/10.1007/s11090-008-9143-1

Gharib-Abou, S., Assadi, A.A., Costa, G., Bouzaza, A., Wolbert, D., 2016. Association of surface dielectric barrier discharge and photocatalysis in continuous reactor at pilot scale: Butyraldehyde oxidation, by-products identification and ozone valorization. Chem. Engin. J. 292, 276-283. https://doi.org/10.1016/j.cej.2016.02.029

Ghodbane, H., Hamdaoui, O., Vandamme, J., Van Durme, J., Vanraes, P., Leys, C., Nikiforov, A.Y., 2014. Degradation of AB25 dye in liquid medium by atmospheric pressure non-thermal plasma and plasma combination with photocatalyst TiO_2, Open Chem. 13, 325–331. https://doi.org/10.1515/chem-2015-0040

Goldstein, S., Merényi, G., 2008. The Chemistry of Peroxynitrite: Implications for Biological Activity. Methods Enzymol. 436, 49-61. https://doi.org/10.1016/S0076-6879(08)36004-2

Gurol, C., Ekinci, F.Y., Aslan, N., Korachi, M., 2012. Low temperature plasma for decontamination of E. coli in milk. Int. J. Food Microbiol. 157, 1–5. https://doi.org/10.1016/j.ijfoodmicro.2012.02.016

Hamrouni, A., Azzouzi, H., Rayes, A., Palmisano, L., Ceccato, R., Parrino, F., 2020. Enhanced solar light photocatalytic activity of ag doped TiO_2-Ag_3PO_4 composites. Nanomaterials. 10, 795. https://doi.org/10.3390/nano10040795.

He, D., Sun, Y., Xin, L., Feng, J., 2014. Aqueous tetracycline degradation by non-thermal plasma combined with nano-TiO_2. Chem. Eng. J. 258, 18-25. https://doi.org/10.1016/j.cej.2014.07.089

Jiang, J., Tan, Z., Shan, C., Pan, J., Pan, G., Liu, Y., Chen, X., Wang, X., 2016. A new study on the penetration of reactive species in their mass transfer processes in water by increasing the electron energy in plasmas. Phys. Plasmas. 23, 103503. https://doi.org/10.1063/1.4964364

Khan, A.U., Kovacic, D., Kolbanovskiy, A., Desai, M., Frenkel, K., Geacintov, N.E., 2000. The ecomposition of peroxynitrite to nitroxyl anion (NO^-) and singlet oxygen in aqueous solution. PNAS. 97, 2984–2989. https://doi.org/10.1073/pnas.97.7.2984

Kim, Y., Choi, Y., Kim, S., Park, J., Chung, M., Song, K.B., Hwang, I., Kwon, K., Park, J., 2009. Disinfection of iceberg lettuce by titanium dioxide–UV photocatalytic reaction. J. Food Prot. 72, 1916–1922. https://doi.org/10.4315/0362-028x-72.9.1916

Kumar, J., Bansal, A., 2013. Photocatalysis by nanoparticles of titanium dioxide for drinking water purification: a conceptual and state-of-art review. Mater. Sci. Forum. 764, 130-150. https://doi.org/10.4028/www.scientific.net/MSF.764.130

Leduc, M., Guay, D., Coulombe, S., Leask, R.L., 2010. Effects of non-thermal plasmas on DNA and mammalian cells. Plasma Process. Polym. 7, 899–909. https://doi.org/10.1002/ppap.201000032

Liu, D.X., Liu, Z.C., Chen, C., Yang, A.J., Li, D., Rong, M.Z., Chen, H.L., Kong, M.G., 2016. Aqueous reactive species induced by a surface air discharge: Heterogeneous mass transfer and liquid chemistry pathways. Sci. Rep. 6, 23737. https://doi.org/10.1038/srep23737

Liu, F., Sun, P., Bai, N., Tian, Y., Zhou, H., Wei, S., Zhou, Y., Zhang, J., Zhou, W., Becker, K., Fang, J., 2010. Inactivation of bacteria in an aqueous environment by a direct-current, cold-atmospheric-pressure air plasma microjet. Plasma Process. Polym. 7, 231–236. https://doi.org/10.1002/ppap.200900070

Lubansky, A.S., Yeow, Y.L., Leong, Y.-K., Wickramasinghe, S.R., Han, B., 2006. A general method of computing the derivate of experimental data. AIChE J. 52, 323–332. https://doi.org/10.1002/aic.10583

Lukes, P., Clupek, M., Sunka, P., Peterka, F., Sano, T., Negishi, N., Matsuzawa, S., Takeuchi, K., 2005. Degradation of phenol by underwater pulsed corona discharge in combination with TiO_2 photocatalysis, Res. Chem. Intermed. 31, 285–294. https://doi.org/10.1163/1568567053956734

Lukes, P., Locke, B.R., Brisset, J.-L., 2012. Aqueous-phase chemistry of electrical discharge plasma in water and in gas–liquid environments, in: Parvulescu, V. I., Magureanu, M., Lukes, P. (Eds.), Plasma chemistry and catalysis in gases and liquids, Wiley-VCH, Weinheim, pp. 243–308.

Martinez, G.R., Di Mascio, P., Bonini, M.G., Augusto, O., Briviba, K., Sies, H., Maurer, P., Roethlisberger, U., Herold, S., Koppenol, W.H., 2000. Peroxynitrite does not decompose to singlet oxygen ($^1\Delta gO_2$) and nitroxyl (NO^-). PNAS. 97, 10307–10312. https://doi.org/10.1073/pnas.190256897

Mei, D., Zhu, X., Chunfei, W., Ashford, B., Williams, P.T., Tu, X., 2016. Plasma-photocatalytic conversion of CO_2 at low temperatures: Understanding the synergistic effect of plasma-catalysis. App. Catal. B: Environ. 182, 552-553. https://doi.org/10.1016/j.apcatb.2015.09.052

643 Meireles, A., Giaouris, E., Simões, M., 2016. Alternative disinfection methods to chlorine for use in
644 the fresh-cut industry. Food Res. Int. 82, 71-85. https://doi.org/10.1016/j.foodres.2016.01.021
645
646 Misra, N.N., Schlüter, O., Cullen, P. J., 2016. Cold plasma in food and agriculture: Fundamentals
647 and applications, Academic Press, Amsterdam., https://doi.org/10.1016/C2014-0-00009-3
648
649 Mitoraj, D., Lamdab U., Kangwansupamonkon, W., Pacia, M., Macyk, W., Wetchakun, N.,
650 Beranek, R., 2018. Revisiting the problem of using methylene blue as a model pollutant in
651 photocatalysis: The case of $InVO_4/BiVO_4$ composites. J. Photochem. Photobiol. A: Chem. 366,
652 103-110. https://doi.org/10.1016/j.jphotochem.2018.02.023
653
654 Moreau, M., Feuilloley, M.G.J., Veron, W., Meylheuc, T., Chevalier, S., Brisset, J.-L., Orange, N.,
655 2007. Gliding arc discharge in the potato pathogen Erwinia carotovora subsp. atroseptica: Mechanism
656 of lethal action and effect on membrane-associated molecules. Appl. Environ. Microbiol. 73, 5904–
657 5910. https://doi.org/10.1128/AEM.00662-07
658
659 Moreau, M., Orange, N., Feuilloley, M., 2008. Non-thermal plasma technologies: new tools for bio-
660 decontamination. Biotechnol. Adv. 26, 610–617. https://doi.org/10.1016/j.biotechadv.2008.08.001
661 Ochiai, T., Hayashi, Y., Ito, M., Nakata, K., Murakami, T., Morito, Y., Fujishima, A., 2012. An
662 effective method for a separation of smoking area by using novel photocatalysis-plasma synergistic
663 air-cleaner. Chem. Engin. J. 209, 313-317. https://doi.org/10.1016/j.cej.2012.07.139
664 Palau, J., Assadi, A.A., Penya-roja, J.M., Bouzaza, A., Wolbert, D., Martínez-Soria, V., 2015.
665 Isovaleraldehyde degradation using UV photocatalytic and dielectric barrier discharge reactors, and
666 their combinations. J. Photochem. Photobiol. A: Chem. 299, 110-117.
667 https://doi.org/10.1016/j.jphotochem.2014.11.013
668 Parrino, F., Camera-Roda, F., Loddo, V., Palmisano, L., 2016. Elemental bromine production by TiO_2
669 photocatalysis and/or ozonation. Angew. Chem. Int. Ed. 55, 0391-10395.
670 https://doi.org/10.1002/anie.201603635
671
672 Parrino, F., Camera-Roda, G., Loddo, V., Augugliaro, V., Palmisano, L., 2013. Photocatalytic
673 ozonation: Maximization of the reaction rate and control of undesired by-products. App. Catal. B:
674 Environ. 178, 37-43. http://dx.doi.org/10.1016/j.apcatb.2014.10.081
675
676 Parrino, F., Conte, P., De Pasquale, C, Laudicina, V.A., Loddo, V., Palmisano, L., 2017. Influence of
677 adsorbed water on the activation energy of model photocatalytic reactions. J. Phys. Chem. C 121, 4,
678 2258–2267. https://doi.org/10.1021/acs.jpcc.6b11945
679
680 Parrino, F., Corsino, S.F., Bellardita, M., Loddo, V., Palmisano, L., Torregrossa, M., Viviani, G.,
681 2019b. Sequential biological and photocatalysis based treatments for shipboard slop purification: A
682 pilot plant investigation. Process Saf. Environ. Prot. 125, 288-296.
683 https://doi.org/10.1016/j.psep.2019.03.025
684
685 Parrino, F., De Pasquale, C., Palmisano, L., 2019. Influence of surface-related phenomena on
686 mechanism, selectivity, and conversion of TiO_2-induced photocatalytic reactions, ChemSusChem.
687 12, 589-602. https://doi.org/10.1002/cssc.201801898
688

689 Parrino, F., Livraghi, S., Giamello, E., Palmisano, L., 2018. The existence of nitrate radicals in
690 irradiated TiO$_2$ aqueous suspensions in the presence of nitrate ions. Angew. Chem. Int. Ed. 57,
691 10702-10706. https://doi.org/10.1002/anie.201804879

692 Parrino, F., Loddo, V., Augugliaro, V., Camera-Roda, G., Palmisano, G., Palmisano, L., 2019.
693 Heterogeneous photocatalysis: guidelines on experimental setup, catalyst characterization,
694 interpretation, and assessment of reactivity, Catal. Rev. Sci. Eng. 61, 163-213.
695 https://doi.org/10.1080/01614940.2018.1546445

696 Pavlovich, M.J., Chang, H.-W., Sakiyama, Y., Clark, D.S., Graves, D.B., 2013. Ozone correlates with
697 antibacterial effects from indirect air dielectric barrier discharge treatment of water. J. Phys. D: Appl.
698 Phys. 46, 145202. https://doi.org/10.1088/0022-3727/46/14/145202
699
700 Perinban, S., Orsat, V., Raghavan, V., 2019. Nonthermal plasma–liquid interactions in food
701 processing: A review. Comp. Rev. Food Sci. F. 18, 1985-2008. https://doi.org/10.1111/1541-
702 4337.12503
703
704 Ragni, L., Berardinelli, A., Iaccheri, E., Gozzi, G., Cevoli, C., Vannini, L., 2016. Influence of the
705 electrode material on the decontamination efficacy of dielectric barrier discharge gas plasma
706 treatments towards *Listeria monocytogenes* and *Escherichia coli*. Innov. Food Sci. Emerg. Technol.
707 37, 170–176. https://doi.org/10.1016/j.ifset.2016.07.029
708
709 Ragni, L., Berardinelli, A., Vannini, L., Montanari, C., Sirri, F., Guerzoni, M.E., Guarnieri, A., 2010.
710 Non-thermal atmospheric gas plasma device for surface decontamination of shell eggs. J. Food Eng.
711 100, 125–132. https://doi.org/10.1016/j.jfoodeng.2010.03.036
712
713 Ryu, J., Choi, W., 2008. Substrate-specific photocatalytic activities of TiO$_2$ and multiactivity test for
714 water treatment application. Environ. Sci. Technol. 42, 1, 294–300.
715 https://doi.org/10.1021/es071470x

716 Saha, A., Goldstein, S., Cabelli, D., Czapski, G., 1998. Determination of optimal conditions for
717 synthesis of peroxynitrite by mixing acidified hydrogen peroxide with nitrite. Free Radic. Biol.
718 Med. 24, 653-639. https://doi.org/10.1016/s0891-5849(97)00365-1

719 Satuf, M.L., Brandi, R.J., Cassano, A.E., Alfano, O.M., 2005. Experimental method to evaluate the
720 optical properties of aqueous titanium dioxide suspensions. Ind. Eng. Chem. Res. 44, 6643-6649.
721 https://doi.org/10.1021/ie050365y
722
723 Selma, M.V., Allende, A., López-Gálvez, F., Conesa, M.Á., Gil, M.I., 2008. Heterogeneous
724 photocatalytic disinfection of wash waters from the fresh-cut vegetable industry, J. Food Prot. 71,
725 286–292. https://doi.org/10.4315/0362-028x-71.2.286
726
727 Shen, J., Tian, Y., Li, Y., Ma, R., Zhang, Q., Zhang, J., Fanf, J., 2016. Bactericidal effects against S.
728 aureus and physicochemical properties of plasma activated water stored at different temperatures. Sci.
729 Rep. 6, 28505. https://doi.org/10.1038/srep28505

730 Sun, P., Wu, H., Bai, N., Zhou, H., Wang, R., Feng, H., Zhou, W., Zhang, J., Fang, J., 2012.
731 Inactivation of Bacillus subtilis spores in water by a direct-current, cold atmospheric-pressure air
732 plasma microjet. Plasma Process. Polym. 9, 157–164. https://doi.org/10.1002/ppap.201100041

Tang, S., Yuan, D., Rao, Y., Zhang, J., Qu, Y., Gu, J., 2018. Evaluation of antibiotic oxytetracycline removal in water using a gas phase dielectric barrier discharge plasma. Journal Environ. Manage. 226, 22–29. https://doi.org/10.1016/j.jenvman.2018.08.022

Tarabová, B., Lukeš, P., Hammer, M.U., Jablonowski, H., von Woedtke, T., Reuter, S., Machala, Z., 2019. Fluorescence measurements of peroxynitrite/peroxynitrous acid in cold air plasma treated aqueous solutions. Phys. Chem. Chem. Phys. 21, 8883-8896. https://doi.org/10.1039/C9CP00871C

Thøgersen, J., Kissner, R., Nauser, T., Koppenol, W.H., Richter, B., Jensen, F., Keiding, S.R., Knak Jensen, S.J., 2015. Primary photochemistry of peroxynitrite in aqueous solution. Chem. Phys. Letters. 641, 187–192. https://doi.org/10.1016/j.cplett.2015.10.056

Tian, W., Kushner, M.J., 2014. Atmospheric pressure dielectric barrier discharges interacting with liquid covered tissue. J. Phys. D: Appl. Phys. 47, 165201. https://doi.org/10.1088/0022-3727/47/16/165201

Tian, Y., Ma, R., Zhang, Q., Feng, H., Liang, Y., Zhang, J., Fang, J., 2015. Assessment of the physicochemical properties and biological effects of water activated by non-thermal plasma above and beneath the water surface, Plasma Process. Polym. 12, 439–449. https://doi.org/10.1002/ppap.201400082

Toledano Garcia, D., Ozer, L.Y., Parrino, F., Ahmed, M., Brudecki, G.P., Hasan, S.W., Palmisano, G., 2018. Photocatalytic ozonation under visible light for the remediation of water effluents and its integration with an electro-membrane bioreactor. Chemosphere 209, 534-541. http://dx.doi.org/10.1016/j.chemosphere.2018.05.197

Vorontsov, A.V., Lyulyukin, M.N., Besov, A. S., 2012. Abatement of air pollutants in combined plasma and photocatalytic systems, Global J. Environ. Sci. Technol. 2, 3.

Wolfe, W.C., 1962. Spectrophotometric determination of hydrogen peroxide in diethyl ether. Anal. Chem. 34, 1328-1330. https://doi.org/10.1021/ac60190a040

Yan, X., Ohno, T., Nishijima, K., Abe, R., Ohtani, B., 2006. Is Methylene Blue an appropriate substrate for a photocatalytic activity test? A study with visible-light responsive titania, Chem. Phys. Lett. 429, 606-610. https://doi.org/10.1016/j.cplett.2006.08.081

Yeow, Y.L, Wickramasinghe, S.R., Han, B., Leong, Y.-K., 2003. A new method of processing the time-concentration data of reaction kinetics. Chem. Eng. Sci. 58, 3601–3610. https://doi.org/10.1016/S0009-2509(03)00263-X

Yousfi, M., Merbahi, N., Sarrette, J.P., Eichwald, O., Ricard, A., Gardou, J.P., Benhenni, M., 2011. Non thermal plasma sources of production of active species for biomedical uses: Analyses, optimization and prospect, in: Fazel-Rezai, R. (Eds.), Biomedical engineering-frontiers and challenges, InTech, Rijeka, pp. 99–124.

Yusupov, M., Neyts, E.C., Simon, P., Berdiyorov, G., Snoeckx, R., Van Duin, A.C.T., Bogaerts, A., 2013. Reactive molecular dynamics simulations of oxygen species in a liquid water layer of interest for plasma medicine. J. Phys. D: Appl. Phys. 47, 025205. https://doi.org/10.1088/0022-3727/47/2/025205

779 Zadi, T., Assadi, A., Nasrallah, N., Bouallouche, R., Nguyen-Tri, P., Bouzaza, A., Azizi, M., Maachi,
780 R., Wolbert, D., Assadi, A., 2018. Treatment of hospital indoor air by a hybrid system of combined
781 plasma with photocatalysis: Case of trichloromethane, an hybrid system of combined plasma with
782 photocatalysis for treatment of hospital indoor air. Chem. Eng. J. 349, 276-286.
783 https://doi.org/10.1016/j.cej.2018.05.073

784 Zhou, R., Zhou, R., Prasad, K., Fang, Z., Speight, R., Bazaka, K., Ostrikov, K.K., 2018. Cold
785 atmospheric plasma activated water as a prospective disinfectant: The crucial role of peroxynitrite.
786 Green Chem. 20, 5276–5284. https://doi.org/10.1039/C8GC02800A

787 Zhou, R., Zhou, R., Zhang, X., Li., J., Wang, X., Chen, Q., Yang, S., Chen, Z., Bazaka, K., Ostrikov,
788 K., 2016. Synergistic Effect of Atmospheric-pressure Plasma and TiO_2 Photocatalysis on Inactivation
789 of Escherichia coli Cells in Aqueous Media, Sci. Rep. 6, 39552. https://doi.org/10.1038/srep39552

790 Zhou, R., Zhou, R., Zhang, X., Zhuang, J., Yang, S., Bazaka, K., Ostrikov, K., 2016b. Effects of
791 atmospheric-pressure N_2, He, air, and O_2 microplasmas on Mung Bean seed germination and seedling
792 growth. Sci. Rep. 6, 32603. https://doi.org/10.1038/srep32603

793 Zhu, Z., Cai, H., Sun, D.-W., 2018. Titanium dioxide (TiO_2) photocatalysis technology for
794 nonthermal inactivation of microorganisms in foods. Trends Food Sci. Tech. 75, 23-35.
795 https://doi.org/10.1016/j.tifs.2018.02.018
796